Rod Photoreceptor Loss in Rho$^{-/-}$ Mice Reduces Retinal Hypoxia and Hypoxia-Regulated Gene Expression

Tanyth E. de Gooyer,[1] *Kathryn A. Stevenson,*[1] *Pete Humphries,*[2] *David A. C. Simpson,*[1] *Timothy M. Curtis,*[1] *Tom A. Gardiner,*[1] *and Alan W. Stitt*[1]

Purpose. This study was conducted to evaluate whether regions of the retinal neuropile become hypoxic during periods of high oxygen consumption and whether depletion of the outer retina reduces hypoxia and related changes in gene expression.

Methods. Retinas from rhodopsin knockout (Rho$^{-/-}$) mice were evaluated along with those of wild-type (WT) control animals. Retinas were also examined at the end of 12-hour dark or light periods, and a separate group was treated with L-*cis*-diltiazem at the beginning of a 12-hour dark period. Hypoxia was assessed by deposition of hypoxyprobe (HP) and HP-protein adducts were localized by immunohistochemistry and quantified using ELISA. Also, hypoxia-regulated gene expression and transcriptional activity were assessed alongside vascular density.

Results. Hypoxia was observed in the inner nuclear and ganglion cell layers in WT retina and was significantly reduced in Rho$^{-/-}$ mice ($P < 0.05$). Retinal hypoxia was significantly increased during dark adaptation in WT mice ($P < 0.05$), whereas no change was observed in Rho$^{-/-}$ or with L-*cis*-diltiazem–treated WT mice. Hypoxia-inducible factor (HIF)-1α DNA-binding and VEGF mRNA expression in Rho$^{-/-}$ retina was significantly reduced in unison with outer retinal depletion ($P < 0.05$). Retina from the Rho$^{-/-}$ mice displayed an extensive intraretinal vascular network after 6 months, although there was evidence that capillary density was depleted in comparison with that in WT retinas.

Conclusions. Relative hypoxia occurs in the inner retina especially during dark adaptation. Photoreceptor loss reduces retinal oxygen usage and hypoxia which corresponds with attenuation of the retinal microvasculature. These studies suggest that in normal physiological conditions and diurnal cycles the adult retina exists in a state of borderline hypoxia, making this tissue particularly susceptible to even subtle reductions in perfusion. (*Invest Ophthalmol Vis Sci.* 2006;47:5553–5560) DOI:10.1167/iovs.06-0646

Oxygenation of the inner retina is achieved through the intraretinal microvasculature, whereas the choriocapillaris supplies the retinal pigment epithelium (RPE) and photoreceptors. The different vascular supply networks create an uneven oxygen tension across the retina with a marked reduction in oxygenation occurring at the level of the outer plexiform layer (OPL).[1–3] Oxygen fluctuation across the retinal layers is related to both the differing capillary densities and disparity in oxygen usage by various retinal neurons and glia.[4] Indeed, the high metabolic demands of the photoreceptors in combination with the characteristic dark adaptation response may make these cells ultrahigh users of retinal oxygen.[4–8]

During dark adaptation, the rod photoreceptors recover their high cytoplasmic calcium levels via cGMP-gated calcium channels with concomitant extrusion of sodium and water. This is a very ATP-dependent process, and it has been estimated that these retinal neurons consume up to four times more oxygen under scotopic, compared with photopic conditions.[4,9] Even in healthy individuals, this dark cycle results in relative depletion of oxygen in the inner retinal layers.[4,8] In patients with retinitis pigmentosa (RP), the loss of rod photoreceptors would be expected to result in reduced metabolic demand and a net reduction in retinal oxygen consumption,[10] although it remains to be determined whether dark adaptation leads to significant retinal hypoxia and whether this alters gene transcription.

Local oxygen tension can significantly affect the retina and its microvasculature by regulation of an array of vasoactive agents including vascular endothelial growth factor (VEGF).[11] Expression of such genes is controlled, in part, by the transcription factor hypoxia-inducible factor (HIF)-1α.[12] VEGF expression in response to physiological hypoxia has been identified as a key regulator of retinal vascular development,[13,14] whereas its inhibition by hyperoxia and overexpression in pathologic hypoxia and variable oxygenation are associated with various disease states.[11,15–17]

Progressive retinal microvascular attenuation is a hallmark feature of patients with RP.[18] This pathologic characteristic is also evident in murine models of RP, in which the retinal microvascular tree shows capillary loss[10] progressive narrowing of vessels,[19] and perhaps some evidence of abnormal vascular development.[20] Mice with photoreceptor loss which are subjected to hyperoxia-induced retinal ischemia display a reduced neovascular response in comparison to controls with full-thickness outer retina,[21] whereas spontaneous regression of optic disc neovascularization has been shown in patients with RP.[22,23] These studies suggest that the outer retina contributes to retinal hypoxia and exacerbates certain diseases in which oxygen deprivation is an important causative factor. However, this hypothesis has not been adequately addressed. With the use of murine models, the current investigation defined the extent of physiological hypoxia that occurs during periods of high oxygen consumption (such as dark adaptation) and after progressive outer retinal depletion, as occurs during RP.

From the [1]Centre for Vision Science, Queen's University Belfast, Royal Victoria Hospital, Belfast, Northern Ireland, United Kingdom; and [2]The Ocular Genetics Unit, Smurfit Institute, Department of Genetics, Trinity College Dublin, Dublin, Ireland.

Supported by Action Medical Research (UK), the Wellcome Trust (UK), and the Juvenile Diabetes Research Fund (USA).

Submitted for publication June 14, 2006; revised August 1, 2006; accepted October 10, 2006.

Disclosure: **T.E. de Gooyer**, None; **K.A. Stevenson**, None; **P. Humphries**, None; **D.A.C. Simpson**, None; **T.M. Curtis**, None; **T.A. Gardiner**, None; **A.W. Stitt**, None

The publication costs of this article were defrayed in part by page charge payment. This article must therefore be marked "*advertisement*" in accordance with 18 U.S.C. §1734 solely to indicate this fact.

Corresponding author: Alan W. Stitt, Centre for Vision Science, Queen's University Belfast, Royal Victoria Hospital, Grosvenor Road, Belfast BT12 6BA, Northern Ireland; a.stitt@qub.ac.uk.

METHODS

Experimental Models

The rhodopsin knockout mouse ($Rho^{-/-}$) displays an RP-like phenotype, with an age-dependent decline in rod number and function.[24] Generated by a replacement mutation in exon 2 of the rhodopsin gene in the C57Bl/6J strain, the mice show reduced outer nuclear layer (ONL) thickness and the absence of a rod ERG response at 48 days of age, with virtually complete rod photoreceptor loss by 3 months. To correlate changes in retinal hypoxia and hypoxia-related gene expression with retinal degeneration, eyes from $Rho^{-/-}$ mice and C57Bl/6 wild-type (WT) control mice were enucleated at 1, 3, and 6 months of age. All procedures were in accordance with the Home Office Animals (Scientific Procedures) Act 1986 and conformed to the ARVO Statement for the Use of Animals in Ophthalmic and Vision Research.

Evaluation of Retinal Morphology

Mice have a rod-rich retina, and the thickness of the ONL is a good indication of rod loss. To evaluate the time course of photoreceptor degeneration in these mice, eyes from $Rho^{-/-}$ mice and C57Bl/6 WT (WT) controls at 1, 3, and 6 months of age were fixed in 4% paraformaldehyde (PFA) for 4 hours, washed in phosphate-buffered saline (PBS) before dehydration, and embedded in wax for sectioning at 5 μm. Hematoxylin and eosin–stained sections were evaluated by light microscopy.

Determination of Retinal Hypoxia

It has been demonstrated that retinal hypoxia can be assessed with the bioreductive drug pimonidazole,[25] which forms irreversible adducts with thiol groups on tissue proteins with $Po_2 < 10$ mm Hg.[26] Groups of $Rho^{-/-}$ and WT mice at 1, 3, and 6 months of age ($n = 6$–8) were given 60 mg/kg pimonidazole (Hypoxyprobe [HP]; Chemicon Europe, Ltd., Chandlers Ford, UK) in sterile water by intraperitoneal injection. After 3 hours, the animals were killed and the eyes enucleated. The right eye from each animal was fixed in 4% PFA for 4 hours and placed in PBS at 4°C before immunofluorescent staining of HP-protein adducts. The neural retina from the left eye was freshly dissected and snap frozen in liquid nitrogen for quantification of HP-protein adducts by indirect competitive ELISA. Retinal wet weights were recorded after collection of retinal tissue samples in preweighed tubes.

For quantification of HP-protein binding, preweighed retinal samples from $Rho^{-/-}$ and WT mice were prepared for an HP competitive ELISA.[27] Snap-frozen retinas were subjected to ultrasonic disruption in RIPA buffer. After centrifugation to remove tissue debris, the protein content of the resultant supernatant was measured using a BCA protein assay kit (Pierce, Rockford, IL). One hundred microliters of sample (45 μg/mL) or standard (0–20 μM) diluted in PBS and 5% Tween 20 were aliquoted in duplicate into a 96-well polystyrene assay plate (Corning-Costar, Inc., Corning, NY) and incubated with 25 μL of rabbit polyclonal antibody against HP (1:3300 in PBS and 5% Tween; kindly donated by James A. Raleigh, University of North Carolina School of Medicine, Chapel Hill, NC) for 1 hour at 37°C. The contents of each well were then transferred to plates (C96 Maxisorp; Nunc International, Roskilde, Denmark) that had been precoated with solid-phase antigen (1:5000 in carbonate buffer; pH 9.6) overnight at 4°C and blocked with 1% gelatin for 1 hour. The competition between solid-phase (HP reductively bound to bovine serum albumin[27]) and soluble antigens proceeded for 1 hour at 37°C, after which the wells were washed four times for 5 minutes each with PBS and 5% Tween and 100 μL 1:2000 alkaline-phosphatase goat anti-rabbit IgG (Sigma-Aldrich, St. Louis, MO) was added to each well. Plates were then washed four times for 5 minutes each with PBS and 5% Tween, and 100 μL of 1 mg/mL of the alkaline-phosphatase substrate 4-nitrophenyl phosphate disodium salt hexahydrate (Sigma-Aldrich) dissolved in 10% diethanolamine buffer (pH 9.6) was added to each well. The color development of the subsequent reaction was measured at 405 nm every 5 minutes for 2 hours on a microplate reader (Safire; Tecan Instruments, Reading, UK) and reaction kinetics analyzed (Magellan ver. 3.11 software; Tecan Instruments). Sample HP binding was determined by comparison to a Lineweaver-Burk enzyme kinetic standard curve, and is expressed as a proportion of sample protein concentration and corrected for retinal tissue weight.

For HP immunolocalization, randomly chosen 5-μm paraffin-embedded sections of 4% PFA–fixed eyes were dewaxed and rehydrated in graded alcohols and water. Sections were then incubated with a 1:1 solution of trypsin and versene (Difco; Sigma-Aldrich) to unmask antigenic regions, washed in distilled H_2O for 10 minutes and incubated for 20 minutes in PBS containing 0.1% Triton X-100 (TX-100) and 10% normal goat serum, to block nonspecific binding of the primary antibody. For visualization of the HP-protein adducts, sections were incubated with an anti-HP rabbit polyclonal antibody (gift from James A. Raleigh) used at a dilution of 1:500 in PBS and 0.1% TX-100, overnight at 4°C. For secondary detection, sections were washed three times in 5-minute changes of PBS, and covered in a 1:500 dilution in PBS and 0.1% TX-100 of a goat anti-rabbit antibody labeled with Alexa-488 (Invitrogen-Molecular Probes Europe BV, Leiden, The Netherlands) for 1 hour at room temperature. Sections were again washed three times in 5 minute changes of PBS, covered with 5 nM of propidium iodide (Sigma-Aldrich) in PBS and 0.1% TX-100 for 20 minutes at room temperature, to visualize cell nuclei. After the sections were washed in PBS for 15 minutes, they were mounted in antifade medium (Vectashield; Vector Laboratories Ltd., Peterborough, UK).

Alternatively, retinal flatmounts were prepared from eyes fixed in 4% PFA for 4 hours which were washed at least overnight in PBS at 4°C. An incision was made 2 mm posterior to the ora serrata, and the anterior segment, lens, and vitreous were removed. The posterior eye cups were relaxed by placing four radial cuts from the retinal periphery to points within 1 mm of the optic disc. The flatmounts were then placed in a 96-well plate in PBS containing 0.3% TX-100 at 4°C overnight to permeabilize the tissue and incubated for 1 hour at 37°C in 10% normal goat serum (Sigma-Aldrich Ltd., Poole, UK) in PBS to block nonspecific binding of the primary antibody. For visualization of the HP-protein adducts an anti-HP rabbit polyclonal antibody (gift from James A. Raleigh) was used at a dilution of 1:50 for 5 hours at 37°C and 100% humidity. This incubation was followed by extensive washing in the permeabilization buffer (six changes) throughout a further 4 hours at 37°C and an additional block with 10% normal goat serum overnight at 4°C. A 1:500 dilution of a goat anti-mouse polyclonal antibody labeled with Alexa-488 (Invitrogen-Molecular Probes Europe BV) was used for secondary detection; the staining time and subsequent washing were as used for the primary antibody. Both retinas of two WT mice were used for immunocytochemical control experiments: Two were stained with the second antibody only and two with nonimmune serum (Vector Laboratories Ltd.) in place of the primary antibody. If nuclear staining was required, retinas were incubated in 5 nM propidium iodide in permeabilization buffer for 10 minutes at 37°C.

Images of stained sections and flatmounts were acquired using a fluorescence microscope (model BX60; Olympus UK Ltd., London, UK) fitted with a confocal scanning laser system (MicroRadiance; BioRad, Herts, UK).

Retinal Hypoxia during Light and Dark Illumination

Additional $Rho^{-/-}$ and WT animals at 3 months of age ($n = 8$–10) were used to assess differences in retinal hypoxia during light and dark adaptation. Animals received an intraperitoneal injection of 60 mg/kg HP at the start of a 12-hour period of light or darkness. A final group of WT animals ($n = 6$) were administered the pharmacological agent L-*cis*-diltiazem (DIL; Biomol Research Laboratories, Plymouth Meeting, PA) which reversibly inhibits the cGMP-activated current of calcium ions, thereby preventing rod cell Ca^{2+} influx and, indirectly, oxygen usage.[28,29] Two intraperitoneal injections of 10 mg/kg DIL (molecular weight 451) in sterile water were administered 2 hours before the commencement of the 12 hours of darkness. Eyes were collected at the

TABLE 1. Total Amount of RNA Extracted per Retina for $Rho^{-/-}$ and WT Samples and Factor Difference

Age (mo)	WT (RNA) (μg/retina)	$Rho^{-/-}$ (RNA) (μg/retina)	Factor Difference
1	2.62	2.13	1.23
3	2.45	1.07	2.29
6	2.48	0.77	3.23

end of these 12-hour periods as described, although in the case of the dark adapted animals, eyes were enucleated and dissected under red light.

Quantitative RT-PCR

Freshly dissected mouse retinas ($n = 8$) were snap frozen in liquid nitrogen. RNA was extracted (Tri Reagent; Sigma-Aldrich), according to the manufacturer's instructions, and purified (RNeasy Mini Kit; Qiagen, Crawley, UK) with residual DNA removed by DNase I digestion (Qiagen). The quantity of RNA in each sample was determined spectrophotometrically (NanoDrop Technologies; LabTech International, Ringmer, UK). RNA samples were reverse transcribed into cDNA (Superscript II RNase H^- reverse transcriptase and a first-strand cDNA synthesis kit; Invitrogen-Life Technologies, Paisley, UK) and random hexamer primers (Roche Molecular Biochemicals, Mannheim, Germany). Real-time reverse transcriptase PCR (RT-PCR) was conducted for quantitative analysis of mRNA expression using murine sequence-specific primers. For normalization of expression data, a 100-bp fragment of 28SrRNA (forward: 5′ TTG AAA ATC CGG GGG AGA G 3′, reverse: 5′ ACA TTG TTC CAA CAT GCC AG 3′) was amplified. Primers used to amplify further murine genes were: a 110-bp fragment of rod photoreceptor specific cGMP phosphodiesterase (*PDE6b*; forward: 5′ TAC CAC AAC TGG CGC CAC 3′, reverse: 5′ GTA ACC ATG GGC AAG GCC 3′; GenBank accession no. NM_008806) and a 189-bp fragment of vascular endothelial growth factor-A (*VEGF-A*), (forward: 5′ TTA CTG CTG TAC CTC CAC C 3′; reverse: 5′ ACA GGA CGG CTT GAA GAT G 3′).[30]

Real-time RT-PCR was performed with a rapid thermal cycler system (LightCycler; Roche Molecular Biochemicals), according to protocols outlined by Simpson et al.[30,31] Briefly, PCR was performed in glass capillary reaction vessels (Roche Molecular Biochemicals) in a 10-μL volume with 0.5 μM primers. Reaction buffer, 2.5 mM $MgCl_2$, dNTPs, *Taq* DNA polymerase (Hotstart), and green fluorescent dye (SYBR Green I) were included in a kit (QuantitTect LightCycler, SYBR Green PCR Master Mix; Qiagen). Amplification of cDNAs involved a 15-minute denaturation step followed by 40 cycles with a 95°C denaturation for 15 seconds, 50°C to 57°C annealing for 20 seconds, and 72°C for an appropriate extension time (10–15 seconds). Fluorescence from the green dye that bound to the PCR product was detected at the end of each 72°C extension period. The specificity of the amplification reactions was confirmed by melting-curve analysis.[31] The quantification data were analyzed with the analysis software that accompanied the thermal cycler (Light Cycler; Roche Molecular Biochemicals), as described previously.[32] Background fluorescence was removed by setting a noise band on the plot of log fluorescence against cycle number. The number of cycles at which the best-fit line through the log-linear portion of each amplification curve intersects the noise band is inversely proportional to the log of copy number.[33] A dilution series of a reference cDNA sample was used to generate a standard curve against which the experimental samples were quantified. For each gene, PCR amplifications were performed in triplicate on at least two independent RT reactions.

As the outer retina is lost in the $Rho^{-/-}$ mice, the relative contributions that surviving cells in the outer retina make to total gene expression differs from that in the WT. The total amount of RNA recovered per retina in $Rho^{-/-}$ was consistently lower than WT and decreased as outer retinal degeneration progressed (Table 1). To account for the loss of outer retina and the disproportionate contribution of inner retina to measurement of gene expression in Rho $^{-/-}$ mice, after normalization to 28s, expression results from these animals were also corrected by the factor difference of the RNA concentration compared to WT.

Transcriptional Activation of HIF-1α

HIF-1α in retinal protein extracts was measured using a commercially available DNA-binding transcription factor ELISA (TransAM HIF-1α; Active Motif Europe, Rixensart, Belgium) which cross reacts with HIF-1α in mouse extracts. Briefly, cell extracts were prepared from freshly dissected snap-frozen retinal samples ($n = 5$–7 retina per group) by mechanical disruption in complete lysis buffer available in the kit. The concentration of protein in the samples was estimated using a bicinchoninic acid (BCA) protein assay kit (Pierce, Rockford, IL). Ten microliters of extract (containing 7 μg of protein) was added to a plate to which an oligonucleotide containing the hypoxia response element (HRE) had been immobilized. A primary antibody directed against HIF-1α was added followed by a secondary HRP-conjugated antibody and HRP substrate. The colorimetric change was measured using a microplate reader (Tecan Instruments) and was directly proportional to the quantity of the HIF-1α present. Extracts incubated in conjunction with WT oligonucleotide were used as the negative control, and nuclear extracts from $CoCl_2$-treated COS-7 cells were used as the positive control.

ADPase Enzyme Histochemistry

Evaluation of the retinal vasculature in whole embedded retina was performed according to the method described by Lutty and McLeod.[34] After overnight fixation of intact eyes in 2% PFA in 0.1 M cacodylate buffer at 4°C, an incision was made 2 mm posterior to the ora serrata, and the anterior segment of the eye was removed. After removal of the vitreous from the eye cup, the retina was carefully separated from the RPE and choroid. The retina was washed in 0.1 M cacodylate buffer with 5% sucrose and then incubated for enzyme histochemical demonstration of adenosine diphosphatase (ADPase) activity. The ADPase-incubated retina was washed in 0.1 M cacodylate buffer with 5% sucrose, and four radial cuts were made from the retinal periphery to points within 1 mm of the optic disc to relax the retina before flat fixing it in one-quarter strength Karnovsky fixative for 72 hours. After three brief washes in 0.1 M cacodylate buffer with 5% sucrose, fixed retina were dehydrated in graded alcohols and flat embedded in resin (JB4; PolySciences Europe, Eppelheim, Germany). Retinal microvascular density was quantified with Image J software (ver. 1.30; available by ftp at http://rsb.info.nih.gov/nih-image; developed by Wayne Rasband, National Institutes of Health, Bethesda, MD) on high-contrast ADPase-labeled flatmounts. A minimum of two fields of view were quantified from each retina in a blinded fashion from six mice.

Statistical Analysis

Data are analyzed (SPSS ver. 11.0; SPSS Inc., Chicago, IL), with one-way analysis of variance (ANOVA) conducted between three or more groups with post hoc analysis made using the Bonferroni multiple-comparisons test. Statistical comparison of data between two groups was made using a *t*-test for independent samples. $P < 0.05$ was considered statistically significant in all cases.

RESULTS

Evaluation of Retinal Morphology and PDE6b Real-Time PCR

Histologic evaluation of retinas from $Rho^{-/-}$ mice revealed a progressive loss of the ONL in comparison to WT mice (Figs. 1A–C). This was evident after 1 month, reduced to approximately three to four cells at 3 months of age with a single layer of nuclei remaining after 6 months. As a complementary eval-

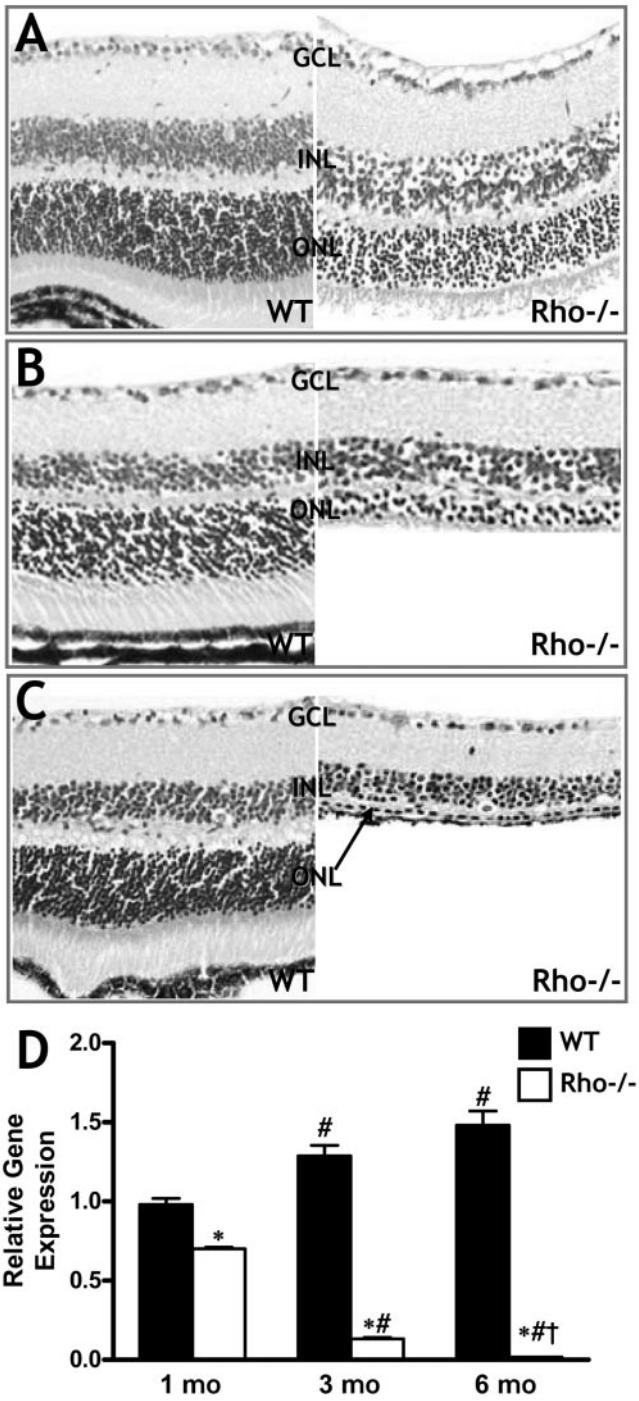

FIGURE 1. Retinal histology and *PDE6b* expression. (**A**) Hematoxylin and eosin (H&E) stained 5-μm paraffin-embedded sections of 1-month-old WT and Rho$^{-/-}$ retina. H&E-stained 5-μm paraffin-embedded sections of (**B**) 3-month-old and (**C**) 6-month-old WT and Rho$^{-/-}$ retinas. The ONL became progressively thinner in Rho$^{-/-}$ retina at 1, 3, and 6 months of age, compared with WT. GCL, ganglion cell layer; INL, inner nuclear layer; ONL, outer nuclear layer. Original magnification, ×40. (**D**) Expression of *PDE6b*, a rod photoreceptor–specific gene, in aged-matched WT and Rho$^{-/-}$. *$P < 0.05$ compared with WT, #$P < 0.05$ compared with 1-month, †$P < 0.05$ compared with 3-month. *PDE6b* expression decreased with age in Rho$^{-/-}$ retina and was significantly lower than WT at 3 and 6 months of age, confirming histologic changes in the outer retina.

uation of rod cell depletion in the Rho$^{-/-}$ mouse, mRNA analysis of phosphodiesterase 6b (PDE6b) as a rod photoreceptor-specific gene was conducted (Fig. 1D). In line with histologic observations, PDE6b mRNA expression was relatively increased at 3 and 6 months of age in WT retina ($P < 0.05$), whereas expression was significantly reduced in the Rho$^{-/-}$ retina with increasing age and progressive ONL loss ($P < 0.05$).

Qualitative and Quantitative Assessment of Retinal Hypoxia

ELISA quantification of HP adducts in WT retina revealed a consistency between 1, 3, and 6 months. This contrasted with HP immunoreactivity levels observed in the Rho$^{-/-}$ retina where there was a stepwise reduction in HP adduct deposition at 3 and 6 months of age compared with aged-matched WT retina with a difference of up to 1.6-fold ($P < 0.05$; Fig. 2A). Immunostaining demonstrated deposition of HP-protein adducts within the cytoplasm of the ganglion cells and cell soma of the inner nuclear layer (INL; Figs. 2C, 2E–G). Intraretinal deposition of HP adducts was reduced in Rho$^{-/-}$ retina at 6 months of age (Fig. 2D) when compared with WT (Fig. 2C).

HP adduct deposition was increased during dark adaptation in the 3-month-old WT retina ($P < 0.05$; Fig. 3A), whereas inhibition of photoreceptor function by treatment with DIL prevented this increase (Fig. 3B). No changes in retinal HP adduct deposition were observed between light exposure and dark adaptation in the Rho$^{-/-}$ retina at 3 months of age (Fig. 3A). Likewise, inhibition of photoreceptor function by treatment with DIL prevented the increase in HP deposition in dark-adapted WT retina (Fig. 3B).

Retinal Transcriptional Activation

Assessment of transcriptional activation by using a protein-DNA binding assay revealed that HIF-1α activity was significantly reduced (1.3-fold) in Rho$^{-/-}$ retina at 6 months (Fig. 4A) compared with that in WT retina and Rho$^{-/-}$ retina at 1 month ($P < 0.05$). Quantitative RT-PCR revealed that VEGF-A gene expression (Fig. 4B) in retinas of Rho$^{-/-}$ mice was reduced with age and was significantly lower than in WT retinas at all ages ($P < 0.05$). This amounted to a reduction of 1.2-fold at 1 month, 1.4-fold at 2 months, and 3.96-fold at 6 months. In WT retinas, expression of VEGF increased at 6 months of age compared with 1 and 3 months ($P < 0.05$).

Assessment of Vascular Density

Darkfield examination of the retinal vasculature in ADPase-reacted flatmounts revealed that in contrast to the dense vascular tree of the WT (Figs. 5A, 5B), retinas from 6-month-old Rho$^{-/-}$ displayed vascular attenuation in the capillary beds (Figs. 5C, 5D). This was most evident proximal to arterioles in the retinal periphery. The arterioles also showed increased tortuosity in regions in which capillary depletion was evident. Such regression of the retinal capillary beds was not as pronounced in sites adjacent to venules (Figs. 5C, 5D). Quantitative image analysis confirmed a significant reduction in retinal vascular density in the Rho$^{-/-}$ animals when compared with WT counterparts ($P < 0.0002$; Fig. 5E).

DISCUSSION

The present study has demonstrated that relative hypoxia occurs in the inner retina of healthy animals, especially during dark adaptation and that this may contribute to the constitutively high levels of VEGF observed in the retina, relative to other tissues. We evaluated retinal oxygenation using the bioreductive drug pimonidazole (HP), which has already been de-

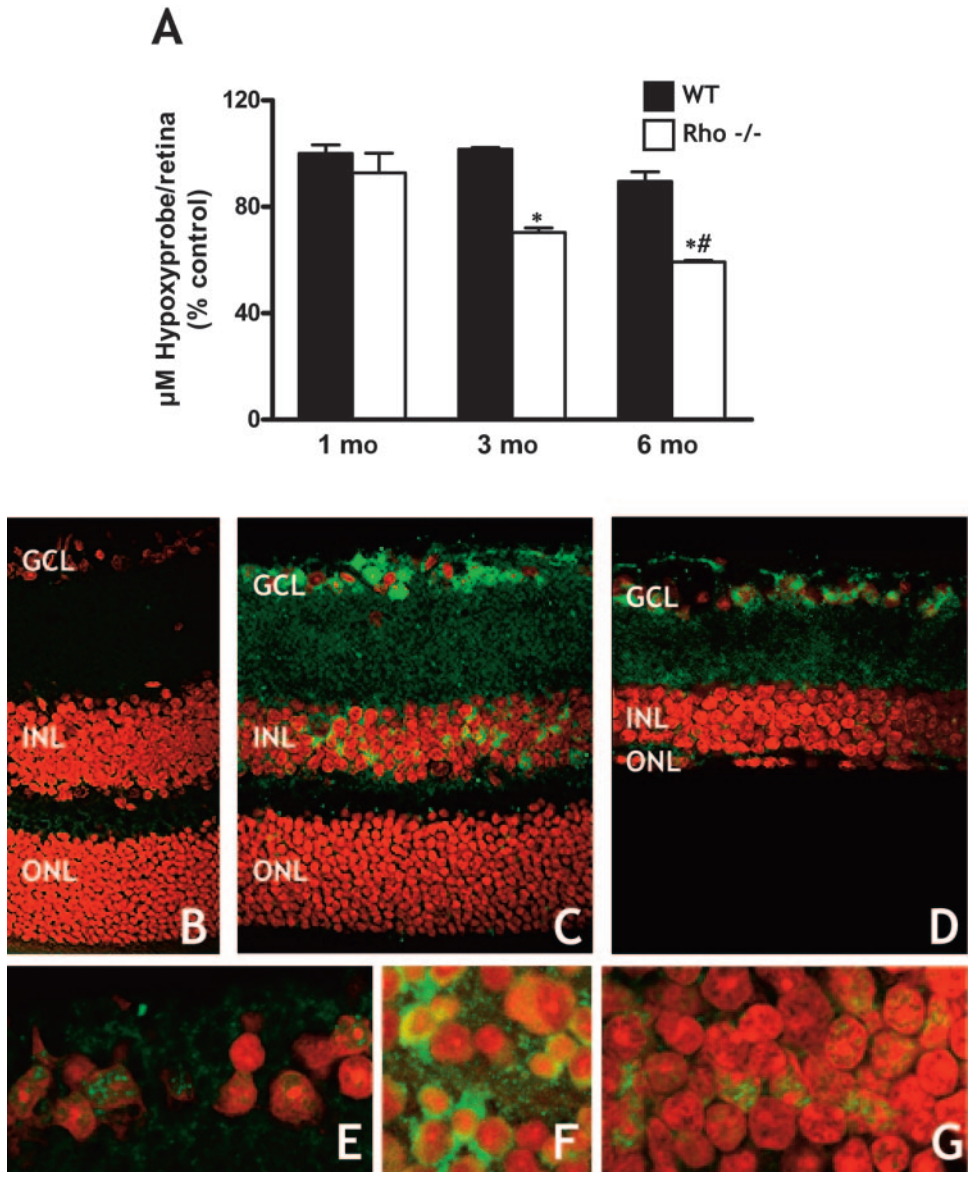

FIGURE 2. Quantitative and qualitative assessment of retinal hypoxia. (**A**) Quantification of retinal hypoxia in aged-matched WT and Rho$^{-/-}$ retina by HP-1-specific ELISA. Retinal hypoxia was significantly reduced in 3- and 6-month-old Rho$^{-/-}$ retinas compared with that in WT retinas. Results expressed as the mean ± SEM. *$P < 0.05$ compared with WT; #$P < 0.05$ compared with 1 month. (**B–G**) Confocal scanning laser micrographs illustrating the localization of hypoxic regions by using immunostaining for HP (represented by *green* fluorescence) in 5-μm paraffin-embedded sections (**B–E**, **G**) and flatmounts (**F**) of retinas from 6-month-old animals. Nuclei of retinal cells are counterstained with propidium iodide (*red* fluorescence). No HP staining was present in the WT nonimmune antisera control (**B**). The WT retina (**C**) was most hypoxic at the level of the GCL and INL, with HP deposits present in the cytoplasm of ganglion cell layers (**E**, **F**) and in the INL (**G**). HP staining appeared to be reduced at these sites in the Rho$^{-/-}$ retina (**D**) compared with WT. GCL, ganglion cell layer; INL, inner nuclear layer; ONL, outer nuclear layer. Original magnification: (**B–D**) ×40; (**E–F**) ×60.

scribed as a reliable indicator of hypoxia in the retina.[25] Early studies of a closely related 2-nitromidazole, pimizonidazole, showed that these drugs have sufficient sensitivity to demonstrate even physiological oxygen gradients in normal liver.[35] This methodology can supplement the invaluable use of oxygen-sensitive microelectrodes because it allows specific localization of hypoxia-sensitive cells in the retina and assessment of larger groups of animals. In the current investigation we have indicated that, under normal conditions, the inner retina from dark-adapted WT mice is relatively hypoxic, with deposition of HP protein adducts localized to the cytoplasm of ganglion cells in particular. It is notable that subpopulations of retinal cells accumulate more HP adducts than others, which may reflect the fact that some cells undergo relatively more intracellular hypoxia. The reason for this is unclear, but ongoing studies of the ischemic retina should determine differentials between retinal cells in terms of oxygen requirements and their susceptibility to hypoxic insult. Ganglion cell deposition of HP may reflect the high metabolic activity of these cells and possibly their efficiency in converting to a more reductive metabolism. Previous investigation has shown that regions of inner retinal ischemia in oxygen-induced retinopathy have intense HP deposition in ganglion cells[25] but not in the adjacent astrocytes, a fact that may be related to survival of the ganglion cells and loss of the astrocytes in such regions.[36,37]

The deposition of HP was reduced as outer retinal degeneration progressed in the light-adapted retina of the Rho$^{-/-}$ mice and this supports similar findings using other methods in the RCS rat[3] and the P23H rat,[38] both of which display reduced retinal hypoxia after photoreceptor loss. It is likely that with fewer photoreceptors acting as a metabolic sink in the Rho$^{-/-}$ mice, oxygen derived from the choroidal circulation more freely diffuses into the inner retina, relieving the hypoxia observed in intact WT retina. Indeed, the choriocapillaris contributes approximately 90% of the oxygen consumed by photoreceptors,[39] and this capillary network shows no evidence of autoregulation, irrespective of oxygen demand.[40] Therefore, in the absence of photoreceptors, excess choroidal oxygen may effectively raise the Po_2 of the inner retina with associated reduction in oxygen-sensitive gene expression and downregulation of vasogenic growth/survival factors such as VEGF.

Further confirmation of the outer retina's contribution to inner retinal hypoxia was provided by the evaluation of retinas from dark-adapted mice. Rod photoreceptor aerobic metabo-

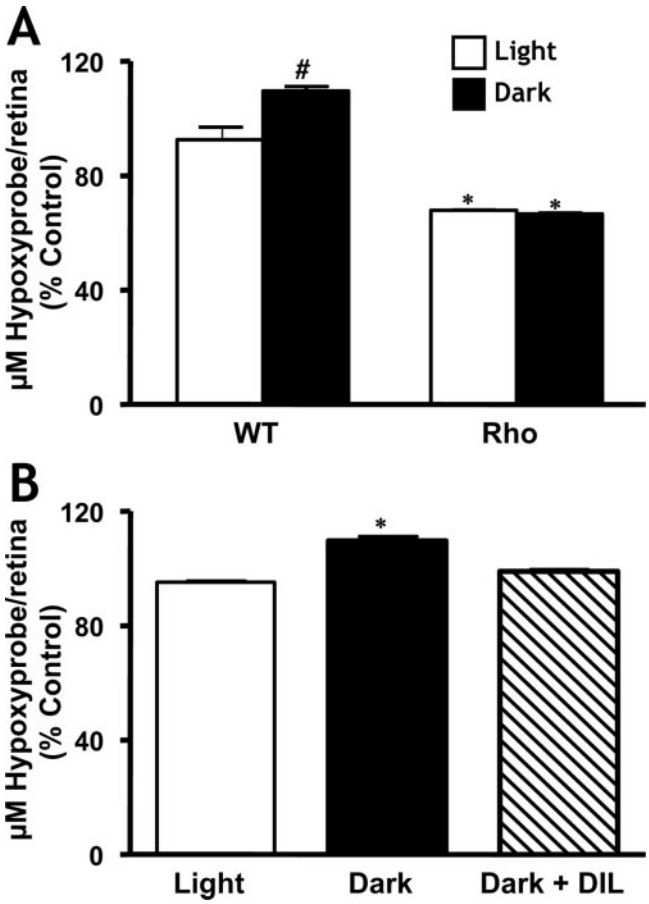

FIGURE 3. Quantitative and qualitative assessment of retinal hypoxia in light- and dark-adapted retina. (**A**) Quantification of retinal hypoxia in 3-month-old light- and dark-adapted WT and $Rho^{-/-}$ retina by HP-specific ELISA. Retinal hypoxia was significantly increased in dark-adapted WT retina. Retinal hypoxia in light-adapted $Rho^{-/-}$ retina was significantly reduced compared with that in WT retina. Because the number of rod photoreceptors is reduced in $Rho^{-/-}$ retinas (Fig. 1), no changes in retinal hypoxia were observed in dark-adapted $Rho^{-/-}$ retinas. Results are expressed as the mean ± SEM. $^{*}P < 0.05$ compared with WT; $^{\#}P < 0.05$ compared with light-adapted. (**B**) Quantification of retinal hypoxia in 3-month-old WT light- and dark-adapted retina after treatment with the specific cGMP calcium channel inhibitor DIL by HP-specific ELISA. The significant increase in retinal hypoxia observed during dark adaptation was prevented by treatment with DIL. Results are expressed as the mean ± SEM. $^{*}P < 0.05$ compared with light-adapted.

lism is known to increase 1.6-fold during dark adaptation in rodents.[41] It has now been demonstrated that this translates to a measurably increased hypoxia in the inner retina and agrees with a related investigation by Cringle et al.[42] using oxygen sensitive microelectrodes. In contrast, the $Rho^{-/-}$ mouse retina with no functional photoreceptors showed no dark adaptation-mediated retinal hypoxia. Moreover, a similar response was induced in the WT retina after inhibition of photoreceptor function using L-*cis*-diltiazem. By blocking the cGMP calcium channels, which are important in establishing the dark current, L-*cis*-diltiazem prevented hypoxia associated with ATPase-dependent Na/K transporters. These findings support both the sensitivity of the HP methodology, and demonstrate the high oxygen usage capacity of the photoreceptor cells.

Retinal oxygen tension has been identified as a key regulator of retinal development and microvascular permeability, growth and survival by altering expression of VEGF,[17,43,44] controlled in part, by cellular oxygen and the transcription factor HIF-1α.[12] In accordance with previous work, the present study has described VEGF to be expressed in the normal adult rodent retina,[45,46] regulated by hypoxia,[47] and reduced when photoreceptors are lost. Dampening VEGF expression can have an impact on pathologic responses by the retina, and it is interesting that when the oxygen-induced proliferative retinopathy model is superimposed on mice with photoreceptor loss there is reduced VEGF-mediated preretinal neovascularization.[48]

Several studies have identified attenuation and abnormalities of the retinal vasculature associated with retinitis pigmentosa in both humans and rodents.[10,18–23] In the present study, vascular attenuation was observed in the juxta-arteriolar capillary beds in the retinal periphery. The mechanism by which atrophic changes in the retinal vasculature of $Rho^{-/-}$ mice accompany advanced photoreceptor degeneration may be the decreased expression of VEGF in these retinas. It is already known that VEGF is a key endothelial survival factor in the

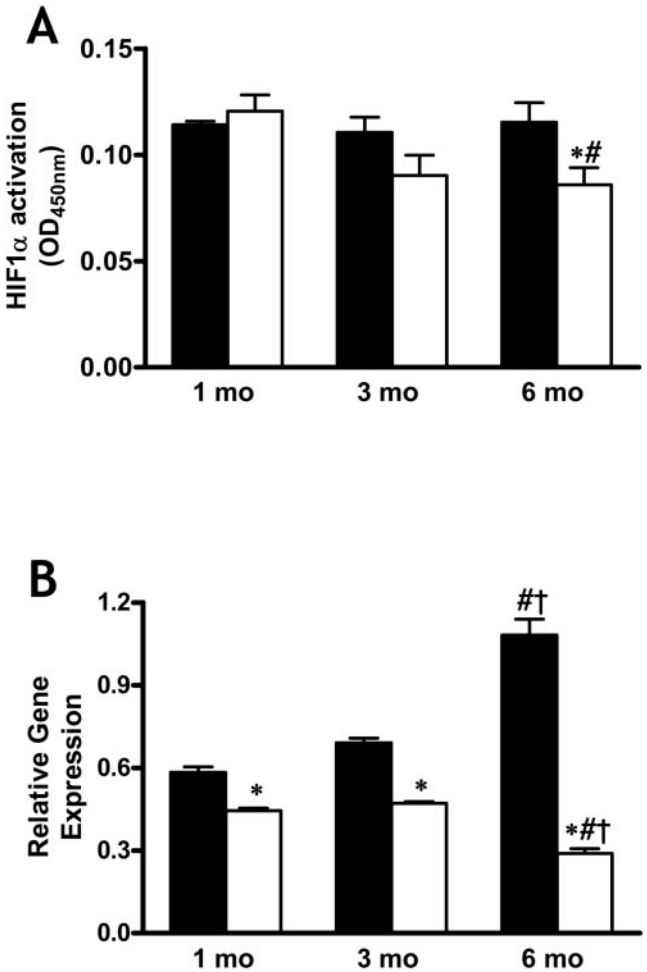

FIGURE 4. HIF-1α activation and VEGF mRNA expression. (**A**) HIF-1α protein-DNA binding in aged-matched WT and $Rho^{-/-}$ retina. In 3- and 6-month-old retinas, HIF-1α expression was significantly lower in $Rho^{-/-}$ retinas compared with 1-month-old and age-matched WT retinas. Results are expressed as the mean ± SEM. $^{*}P < 0.05$ compared with WT; $^{\#}P < 0.05$ compared with 1-month; $^{\dagger}P < 0.05$ compared with 3-month. (**B**) VEGF gene expression in aged-matched WT and $Rho^{-/-}$ retina. VEGF expression increased significantly with age in WT retinas and decreased with age in $Rho^{-/-}$ retinas. In 3- and 6-month-old mice, VEGF expression was significantly lower in $Rho^{-/-}$ compared with WT retinas. Results expressed as mean ± SEM. $^{*}P < 0.05$ compared with WT, $^{\#}P < 0.05$ compared with 1-month; $^{\dagger}P < 0.05$ compared with 3-month.

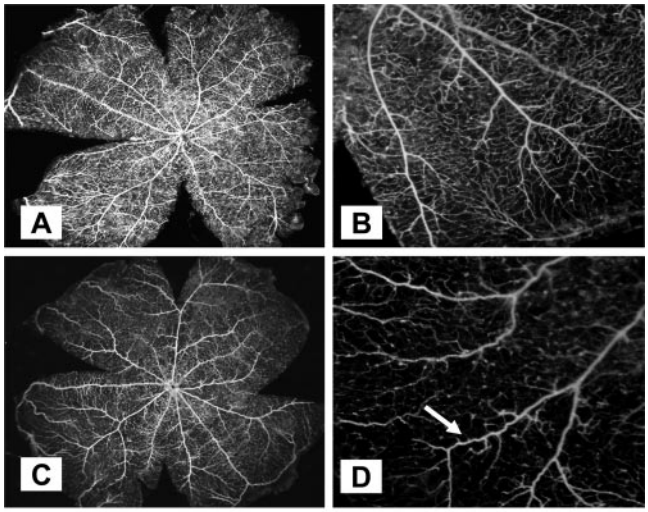

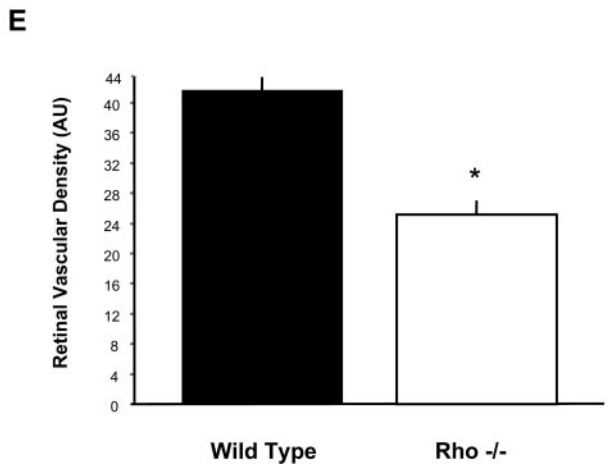

FIGURE 5. Vascular density during photoreceptor depletion in Rho$^{-/-}$. (**A**, **B**) Vasculature visualized by ADPase enzyme histochemistry in 6-month-old WT retina. Images show the dense vasculature in the mid and peripheral regions at low (**A**) and high (**B**) magnification. The microvascular tree in 6-month-old Rho$^{-/-}$ retina displayed vascular attenuation in the capillary beds (**C**, **D**), most evident around arterioles in the retinal periphery (**D**, *arrow*), which also appear tortuous. Quantification of vascular density showed that there was a significant reduction in vasculature in the Rho$^{-/-}$ retina when compared with WT (*$P < 0.0002$). Error bars, SEM. Original magnification: (**A**, **C**) ×3; (**B**, **D**) ×10.

neonatal retina,[49] with endothelial cells undergoing apoptosis when this factor is reduced.[43] The importance of retinal oxygen tension in leading to vascular changes is highlighted in a study by Penn et al.,[10] which demonstrated that low ambient oxygen can reverse capillary atrophy and stimulate new capillary growth in a transgenic mouse model of autosomal dominant RP. Indeed, VEGF expression in response to physiologic hypoxia has been identified as a key regulator of retinal vascular development,[13,14] whereas its inhibition by hyperoxia and overexpression in pathologic hypoxia and variable oxygenation are associated with various disease states.[11,15–17] Local VEGF expression by retinal astrocytes[14,16] represents an important survival factor for retinal vascular endothelial cells[43] and is spatially correlated with the physiological capillary-free zone around retinal arterioles.[16] Claxton and Fruttiger[16] have demonstrated that the juxta-arteriolar area showing reduced VEGF expression is coincident with the capillary-free zone, whereas effective oxygenation of this region has been demonstrated by exclusion of HP in the tissue proximal to retinal arterioles as they traverse ischemic retina during oxygen-induced retinopathy.[25]

This study has demonstrated that relative hypoxia occurs in the normal retina, which may account for constitutively high levels of HIF-1α transcriptional activity and associated increases in VEGF mRNA expression. Photoreceptor loss in RP reduces retinal oxygen usage and subsequent development of relative hypoxia and related gene expression. Although the increases in HIF-1α transcription were relatively small, this may reflect a subpopulation of retinal glia and neurons that subsequently upregulate expression of hypoxia-induced growth factors. Indeed, VEGF expression changes were extensive between some groups. Such regulatory capacity in the retina is physiologically significant, because alteration of the fine balance of such growth/survival factors may have an impact on subsequent attenuation of the retinal vasculature and suggests that outer retinal hypoxia may influence certain diseases where oxygen deprivation is an important etiological factor. Particularly, the mechanisms described in this study provide support for further evaluation of Arden's hypothesis,[28] that loss of photoreceptors during RP may offset the exacerbation of hypoxia during diabetic retinopathy and thereby protect the microvasculature from pathogenic change.

Acknowledgments

The authors thank Matthew Owens for providing technical assistance.

References

1. Alder VA, Cringle SJ. Vitreal and retinal oxygenation. *Graefes Arch Clin Exp Ophthalmol.* 1990;228:151–157.
2. Linsenmeier RA, Goldstick TK, Blum RS, Enroth-Cugell C. Estimation of retinal oxygen transients from measurements made in the vitreous humor. *Exp Eye Res.* 1981;32:369–379.
3. Yu DY, Cringle SJ, Su EN, Yu PK. Intraretinal oxygen levels before and after photoreceptor loss in the RCS rat. *Invest Ophthalmol Vis Sci.* 2000;41:3999–4006.
4. Drasdo N, Chiti Z, Owens DR, North RV. Effect of darkness on inner retinal hypoxia in diabetes. *Lancet.* 2002;359:2251–2253.
5. Braun RD, Linsenmeier RA, Goldstick TK. Oxygen consumption in the inner and outer retina of the cat. *Invest Ophthalmol Vis Sci.* 1995;36:542–554.
6. Linsenmeier RA. Effects of light and darkness on oxygen distribution and consumption in the cat retina. *J Gen Physiol.* 1986;88:521–542.
7. Yu DY, Cringle SJ. Retinal degeneration and local oxygen metabolism. *Exp Eye Res.* 2005;80:745–751.
8. Arden GB, Sidman RL, Arap W, Schlingemann RO. Spare the rod and spoil the eye. *Br J Ophthalmol.* 2005;89:764–769.
9. Braun RD, Linsenmeier RA, Goldstick TK. Oxygen consumption in the inner and outer retina of the cat. *Invest Ophthalmol Vis Sci.* 1995;36:542–554.
10. Penn JS, Li S, Naash MI. Ambient hypoxia reverses retinal vascular attenuation in a transgenic mouse model of autosomal dominant retinitis pigmentosa. *Invest Ophthalmol Vis Sci.* 2000;41:4007–4013.
11. Werdich XQ, McCollum GW, Rajaratnam VS, Penn JS. Variable oxygen and retinal VEGF levels: correlation with incidence and severity of pathology in a rat model of oxygen-induced retinopathy. *Exp Eye Res.* 2004;79:623–630.
12. Dery MA, Michaud MD, Richard DE. Hypoxia-inducible factor 1: regulation by hypoxic and non-hypoxic activators. *Int J Biochem Cell Biol.* 2005;37:535–540.
13. Chan-Ling T, Gock B, Stone J. The effect of oxygen on vasoformative cell division; evidence that "physiological hypoxia" is the stimulus for normal retinal vasculogenesis. *Invest Ophthalmol Vis Sci.* 1995;36:1201–1214.
14. Stone J, Itin A, Alon T, et al. Development of retinal vasculature is mediated by hypoxia-induced vascular endothelial growth factor (VEGF) expression by neuroglia. *J Neurosci.* 1995;15:4738–4747.

15. Simpson DA, Murphy GM, Bhaduri T, et al. Expression of the VEGF gene family during retinal vaso-obliteration and hypoxia. *Biochem Biophys Res Commun*. 1999;262:333–340.
16. Claxton S, Fruttiger M. Role of arteries in oxygen induced vaso-obliteration. *Exp Eye Res.* 2003;77:305–311.
17. Pierce EA, Avery RL, Foley ED, Aiello LP, Smith LE. Vascular endothelial growth factor/vascular permeability factor expression in a mouse model of retinal neovascularization. *Proc Natl Acad Sci USA*. 1995;92:905–909.
18. Milam AH, Li ZY, Fariss RN. Histopathology of the human retina in retinitis pigmentosa. *Prog Retin Eye Res.* 1998;17:175–205.
19. Hawes NL, Smith RS, Chang B, et al. Mouse fundus photography and angiography: a catalogue of normal and mutant phenotypes. *Mol Vis*. 1999;5:22–29.
20. Blanks JC, Johnson LV. Vascular atrophy in the retinal degenerative rd mouse. *J Comp Neurol.* 1986;254:543–553.
21. Lahdenranta J, Pasqualini R, Schlingemann RO, et al. An anti-angiogenic state in mice and humans with retinal photoreceptor cell degeneration. *Proc Natl Acad Sci USA*. 2001;98:10368–10373.
22. To KW, Nadel AJ, Perlstein SH, Margolis S. Bilateral optic disc neovascularization in association with retinitis pigmentosa. *Can J Ophthalmol.* 1991;26:152–155.
23. Hayakawa M, Hotta Y, Imai Y, et al. Clinical features of autosomal dominant retinitis pigmentosa with rhodopsin gene codon 17 mutation and retinal neovascularization in a Japanese patient. *Am J Ophthalmol*. 1993;115:168–173.
24. Humphries MM, Rancourt D, Farrar GJ, et al. Retinopathy induced in mice by targeted disruption of the rhodopsin gene. *Nat Genet*. 1997;15:216–219.
25. Gardiner TA, Gibson DS, de Gooyer TE, et al. Inhibition of tumor necrosis factor-alpha improves physiological angiogenesis and reduces pathological neovascularization in ischemic retinopathy. *Am J Pathol*. 2005;166:637–644.
26. Raleigh JA, Koch CJ. Importance of thiols in the reductive binding of 2-nitroimidazoles to macromolecules. *Biochem Pharmacol.* 1990;40:2457–2464.
27. Raleigh JA, La Dine JK, Cline JM, Thrall DE. An enzyme-linked immunosorbent assay for hypoxia marker binding in tumours. *Br J Cancer.* 1994;69:66–71.
28. Arden GB. The absence of diabetic retinopathy in patients with retinitis pigmentosa: implications for pathophysiology and possible treatment. *Br J Ophthalmol.* 2001;85:366–370.
29. Stern JH, Kaupp UB, MacLeish PR. Control of the light-regulated current in rod photoreceptors by cyclic GMP, calcium, and L-cis-diltiazem. *Proc Natl Acad Sci USA*. 1986;83:1163–1167.
30. Feeney SA, Simpson DA, Gardiner TA, et al. Role of vascular endothelial growth factor and placental growth factors during retinal vascular development and hyaloid regression. *Invest Ophthalmol Vis Sci*. 2003;44:839–847.
31. Simpson DA, Feeney S, Boyle C, Stitt AW. Retinal VEGF mRNA measured by SYBR green I fluorescence: a versatile approach to quantitative PCR. *Mol Vis.* 2000;6:178–183.
32. Morrison TB, Weis JJ, Wittwer CT. Quantification of low-copy transcripts by continuous SYBR Green I monitoring during amplification. *Biotechniques.* 1998;24:954–958, 960, 962.
33. Higuchi R, Fockler C, Dollinger G, Watson R. Kinetic PCR analysis: real-time monitoring of DNA amplification reactions. *Biotechnology.* 1993;11:1026–1030.
34. Lutty GA, McLeod DS. A new technique for visualization of the human retinal vasculature. *Arch Ophthalmol.* 1992;110:267–276.
35. Maxwell AP, MacManus MP, Gardiner TA. Misonidazole binding in murine liver tissue: a marker for cellular hypoxia in vivo. *Gastroenterology.* 1989;97:1300–1303.
36. Chan-Ling T, Stone J. Degeneration of astrocytes in feline retinopathy of prematurity causes failure of the blood-retinal barrier. *Invest Ophthalmol Vis Sci.* 1992;33:2148–2159.
37. Stone J, Chan-Ling T, Pe'er J, et al. Roles of vascular endothelial growth factor and astrocyte degeneration in the genesis of retinopathy of prematurity. *Invest Ophthalmol Vis Sci.* 1996;37:290–299.
38. Yu DY, Cringle S, Valter K, et al. Photoreceptor death, trophic factor expression, retinal oxygen status, and photoreceptor function in the P23H rat. *Invest Ophthalmol Vis Sci*. 2004;45:2013–2019.
39. Linsenmeier RA, Braun RD. Oxygen distribution and consumption in the cat retina during normoxia and hypoxemia. *J Gen Physiol.* 1992;99:177–197.
40. Delaey C, Van De Voorde J. Regulatory mechanisms in the retinal and choroidal circulation. *Ophthalmic Res.* 2000;32:249–256.
41. Medrano CJ, Fox DA. Oxygen consumption in the rat outer and inner retina: light- and pharmacologically-induced inhibition. *Exp Eye Res.* 1995;61:273–284.
42. Cringle SJ, Yu DY, Yu PK, Su EN. Intraretinal oxygen consumption in the rat *in vivo. Invest Ophthalmol Vis Sci.* 2002;43:1922–1927.
43. Alon T, Hemo I, Itin A, et al. Vascular endothelial growth factor acts as a survival factor for newly formed retinal vessels and has implications for retinopathy of prematurity. *Nat Med*. 1995;1:1024–1028.
44. Nomura M, Yamagishi S, Harada S, et al. Possible participation of autocrine and paracrine vascular endothelial growth factors in hypoxia-induced proliferation of endothelial cells and pericytes. *J Biol Chem*. 1995;270:28316–28324.
45. Gao H, Qiao X, Gao R, et al. Intravitreal triamcinolone does not alter basal vascular endothelial growth factor mRNA expression in rat retina. *Vision Res*. 2004;44:349–356.
46. Ozaki H, Yu AY, Della N, et al. Hypoxia inducible factor-1α is increased in ischemic retina: temporal and spatial correlation with VEGF expression. *Invest Ophthalmol Vis Sci*. 1999;40:182–189.
47. Calvert JW, Zhou C, Zhang JH. Transient exposure of rat pups to hyperoxia at normobaric and hyperbaric pressures does not cause retinopathy of prematurity. *Exp Neurol.* 2004;189:150–161.
48. Yamada H, Yamada E, Hackett SF, et al. Hyperoxia causes decreased expression of vascular endothelial growth factor and endothelial cell apoptosis in adult retina. *J Cell Physiol*. 1999;179:149–156.
49. Benjamin LE, Hemo I, Keshet E. A plasticity window for blood vessel remodelling is defined by pericyte coverage of the preformed endothelial network and is regulated by PDGF-B and VEGF. *Development.* 1998;125:1591–1598.